Longitudinal variation in the ionosphere-plasmasphere system at the minimum of solar and geomagnetic activity: Investigation of temporal and latitudinal dependences

Maxim V. Klimenko, Vladimir V. Klimenko, Irina E. Zakharenkova, Artem M. Vesnin, Iurii V. Cherniak, Ivan A. Galkin

AGU PUBLICATIONS

Radio Science

RESEARCH ARTICLE
10.1002/2015RS005900

Special Section:
Ionospheric Effects Symposium 2015

Longitudinal variation in the ionosphere-plasmasphere system at the minimum of solar and geomagnetic activity: Investigation of temporal and latitudinal dependences

Maxim V. Klimenko[1,2], Vladimir V. Klimenko[1], Irina E. Zakharenkova[1,3], Artem M. Vesnin[4], Iurii V. Cherniak[5], and Ivan A. Galkin[6]

[1]West Department of Pushkov Institute of Terrestrial Magnetism, Ionosphere and Radiowave Propagation RAS, Kaliningrad, Russia, [2]The Institute of Physics and Technology, Immanuel Kant Baltic Federal University, Kaliningrad, Russia, [3]Institut de Physique du Globe de Paris, Paris, France, [4]Institute of Solar-Terrestrial Physics SB RAS, Irkutsk, Russia, [5]Space Radio-Diagnostics Research Centre, University of Warmia and Mazury, Olsztyn, Poland, [6]UML Center for Atmospheric Research, University of Massachusetts Lowell, Lowell, Massachusetts, USA

Abstract We use the Global Self-consistent Model of the Thermosphere, Ionosphere and Protonosphere (GSM TIP) as the first-principle calculation of the physical system state, the quick-run ionospheric electron density model (NeQuick) as the climatology background, and the International Reference Ionosphere-based Real-Time Assimilative Model for a global view of the ionospheric weather during a quiet period of the December 2009 solstice. The model computations are compared to the Constellation Observing System for Meteorology, Ionosphere, and Climate (COSMIC) radio occultation profiles, CHAMP and Gravity Recovery and Climate Experiment in situ densities, and GPS total electron content (TEC). It is shown that the plasma density in the ionosphere is generally larger in the American/Atlantic longitudinal sector at any local time. The high-latitude density enhancements are visible in the GSM TIP output at different altitudes but are not reproduced by the NeQuick empirical model. Given that observational data confirm an existence of the high-latitude areas where ionospheric densities are elevated in the altitude range between 300 and 480 km, we conclude that the N_mF_2 maximum in the GSM TIP output can be trusted. Indeed, such high-latitude N_mF_2, ionospheric electron content, and TEC maxima in the American longitude sector form on the proper places as shown by the GSM TIP data, COSMIC and GPS observations. According to our results, the high-latitude maximum of N_mF_2 (1) manifests itself only when the integration over LT or UT of the global maps for 22 December 2009 includes nighttime, i.e., supporting an argument of its close association with the Weddell Sea Anomaly, and (2) also appears in the N_e distribution at altitudes above the F_2 peak.

Key Points:
- Time-averaged N_mF_2 and TEC maxima are formed at almost all latitudes at American/Atlantic longitudes
- Latitude-averaged Ne in the F region/topside ionosphere is generally greater at American longitudes for any LT
- Weddell Sea Anomaly is manifested as high-latitude maximum in N_mF_2 and TEC-averaged global maps

Supporting Information:
- Supporting Information S1

Correspondence to:
M. V. Klimenko,
maksim.klimenko@mail.ru

Citation:
Klimenko, M. V., V. V. Klimenko, I. E. Zakharenkova, A. M. Vesnin, I. V. Cherniak, and I. A. Galkin (2016), Longitudinal variation in the ionosphere-plasmasphere system at the minimum of solar and geomagnetic activity: Investigation of temporal and latitudinal dependences, *Radio Sci.*, *51*, 1864–1875, doi:10.1002/2015RS005900.

Received 1 DEC 2015
Accepted 4 NOV 2016
Accepted article online 10 NOV 2016
Published online 12 DEC 2016

1. Introduction

Plasma in the Earth's ionosphere-plasmasphere system plays the pivotal role in the transionospheric radio waves propagation, in particular for signals of the Global Navigation Satellite Systems (GNSS). In order to model the ionospheric electron density we need to know the typical variations at the quiet conditions. Usually, to determine the typical (diurnal, UT, or longitudinal) variations of the ionospheric parameters at different latitudes, it is necessary to average observations from all available data sets. This approach allows us to reveal the major temporal and spatial features of the ionospheric parameters. The discovered morphology can be used to improve empirical ionospheric models like the International Reference Ionosphere (IRI) model [*Bilitza and Reinisch*, 2008].

Earlier, it was believed that diurnal variations of the ionospheric parameters significantly exceed the longitudinal variations. However, the first satellite observations disproved this hypothesis [*Eccles et al*., 1971]. Our paper presents the longitudinal variations and estimates their contribution to spatiotemporal variations of the ionosphere-plasmasphere system parameters. Regardless of the recent progress in the description of the F_2 layer peak density, N_mF_2, and the total electron content (TEC) longitudinal structure morphology, there are very few papers devoted to the longitudinal variations of N_mF_2 and TEC in different latitudinal regions [*Klimenko et al*., 2016a, 2016b]. One of the investigation where the seasonal variations of the plasmaspheric electron density were studied at the different L shells (L is McIlwain parameter) was reported by *Clilverd et al*. [2007].

In our paper, we report qualitative and quantitative characteristics of the longitudinal variations in N_mF_2, TEC, and the ionospheric electron content (IEC) derived for all local time (LT) and latitudes. We present each of N_mF_2, IEC, and TEC data set normalized to its maximum value in this particular data set. So we focus here on these parameters' variability only, and we do not consider the absolute values derived from the different data sources. We examined the normalized TEC maps for potential artifacts of the biased values present in the data that may expand the true variation range for visual representation; no significant issues were identified with this approach. We analyzed data for the 2009 December solstice conditions, which were characterized by the quiet geomagnetic conditions at the deep minimum of solar activity. We compared observations and the Global Self-consistent Model of the Thermosphere, Ionosphere and Protonosphere (GSM TIP), quick-run ionospheric electron density model (NeQuick), and IRI-based Real-Time Assimilative Mapping (IRTAM) computation results, which allows us to understand these models' performance.

It is often assumed that the TEC and N_mF_2 variations are correlated. This statement is based on an assumption of a small plasmasphere contribution into TEC. However, recent studies demonstrate that (1) N_mF_2 and TEC behavior can be significantly different during a geomagnetic storm especially at a recovery phase [*Cherniak et al*., 2014]; (2) contribution of the topside ionosphere and plasmasphere to TEC results in a shift to earlier hours and weakening of the Midlatitude Summer Evening Anomaly in TEC compared to one in N_mF_2 [*Klimenko et al*., 2015b]; (3) sometimes, the regions above the F_2 layer peak (h_mF_2) provide the major contribution to TEC [*Afraimovich et al*., 2011; *Klimenko et al*., 2015c]. This effect is even more pronounced during nighttime at the solar activity minimum, where the plasmaspheric contribution to TEC can exceed the ionospheric one [*Lunt et al*., 1999a, 1999b; *Cherniak et al*., 2012; *Klimenko et al*., 2015c]. We address the following problem in our study: can we use the N_mF_2 spatial structure to construct a model of TEC, and vice versa can diurnal (LT) and longitudinal variations of TEC reduced from a ground-based network of GPS receivers be applied to describe the F_2 layer parameters?

2. Observation Data Description

We use simulated and measured N_mF_2 and TEC to study the diurnal, UT, and latitudinal and longitudinal variations. The spatiotemporal distribution of the electron density in the ionosphere and plasmasphere can be represented as a function "*f*" of time and space. When we consider nonstationary processes and spherical geographic coordinate system this function becomes $f(r, \theta, \lambda, t)$, where r is a radius vector drawn from the center of the Earth to a given point, θ is a colatitude or a polar angle measured from the geographical North Pole, $\theta = 90° - \phi$, ϕ is a latitude, measured from the geographical equator, λ is a geographic longitude, measured from the Greenwich meridian, and t is time. N_mF_2 and TEC are mapped on globe surface and therefore are functions of latitude ϕ, longitude λ, and time t. Time t is UT or LT. Data integration over all UT or LT times is a technique that provides an insight into the latitude-longitudinal variability of an examined parameter. Similarly, an integration over all longitude or latitude gives us the diurnal variation of the parameter versus latitude or longitude. When data are available on a particular data grid, the integration operation is simply a sum of all values over the integration variable, divided by a number of the data grid nodes. For example, UT/LT integration process sums 24 two-dimensional data sets, point by point, and divides this sum by 24. This approach allows us to aggregate the major spatial and temporal features of N_mF_2 and TEC variations.

We analyzed the absolute TEC data from the International GPS Service (IGS) global ionospheric maps (GIMs) based on data from worldwide network of ground-based GPS/Global Navigation Satellite System (GLONASS) receivers. GIMs have spatial resolution of 5° in longitude and 2.5° in latitude and temporal resolution of 1–2 h. Here we use the final GIM product generated by the IGS center at University of Warmia and Mazury in Olsztyn (file name IGSGddd0.yyi). The final product is a weighted combination of all GIMs produced by Center for Orbit Determination in Europe, European Space Agency, Jet Propulsion Laboratory, and Polytechnical University of Catalonia. We consider this composite GIM product as a more optimal choice for our research between a variety of GIMs from independent IGS centers: all of these maps (built by selecting different subsets of GPS observatories) contribute to calculation of the combined GIM. However, even though the final GIM includes results from all GPS stations used by four independent IGS centers for GIMs processing, it still cannot solve problems with data gaps over oceans and regions with lack of GPS receivers.

Multisatellite measurements were used as an additional data source, which provided information about the ionospheric plasma density at the different altitudes. CHAMP (CHAllenging Minisatellite Payload) satellite is a

German LEO mission with various objectives in scientific research and application. It was launched on 15 July 2000 into a circular, near-polar (inclination is equal 87.3°) orbit with an initial altitude of ~450 km. The orbit altitude was continuously decreasing and became ~315 km in December 2009. Planar Langmuir Probe (PLP) provides in situ measurements of electron density (N_e in el/cm^3) every 15 s.

The Gravity Recovery and Climate Experiment (GRACE)-B satellite follows GRACE-A satellite at a distance of about 220 km. In order to determine in situ electron density we used the *K* band ranging system (KBR), which measures the dual one-way range changes between two satellites. More detailed description of the electron density determination from the GRACE KBR data is presented by *Xiong et al*. [2010]. The GRACE mission orbit altitude was ~480 km at December 2009.

FORMOSAT-3/COSMIC, named hereafter COSMIC, is a joint Taiwan/U.S. mission consisting of six satellites, placed at the orbit altitude of 700–800 km. Each satellite has a GPS Occultation Experiment payload to operate the ionospheric radio occultation (RO) measurements. We used the COSMIC RO measurements to derive the global maps of IEC corresponding to the altitudinal range of 80–700 km. More detailed description of the COSMIC RO data selection and processing is presented by *Cherniak et al*. [2012]. In a similar way, we constructed the COSMIC-derived global maps of N_mF_2 for the December 2009 solstice.

3. GSM TIP Model Brief Description

The GSM TIP model [*Namgaladze et al*., 1988; *Klimenko et al*., 2007] was developed at the WD IZMIRAN (West Department of Pushkov Institute of Terrestrial Magnetism, Ionosphere and Radiowave propagation of the Russian Academy of Sciences, Kaliningrad). It was used for simulations of the time-dependent global structure of the near-Earth space environment from 80 km to 15 Earth radii. In the thermospheric block of the model, global distribution of the neutral gas temperature (T_n) and N_2, O_2, O, NO, N(^{4}S), and N(^{2}D) densities, as well as the three-dimensional circulation of the neutral gas, N_2^+, O_2^+, and NO^+, and also their temperature (T_i) and velocities (V_i), is calculated in the range from 80 to 526 km in a spherical geomagnetic coordinate system. In the ionospheric section of the model the global time-dependent distributions of ion and electron temperatures (T_i, T_e), vector velocity (V_i), and O^+ and H^+ ion concentrations are calculated in a magnetic dipole coordinate system from 175 km in the Southern Hemisphere to 175 km in the Northern Hemisphere. In this case, the ionosphere code for atomic ions does not require an upper boundary condition. The total electron content (TEC) in the GSM TIP model is calculated by integration of the electron density from bottom side ionosphere to the altitude of GPS/GLONASS satellites (20,200 km). Additionally, the model also provides the two-dimensional electric potential distribution of the ionospheric and magnetospheric origin. The Earth's magnetic field is approximated by a tilted dipole.

The GSM TIP model takes into account the mismatch between geographic and geomagnetic axes, as well as dynamical processes in ionosphere-plasmasphere system such as (1) plasma diffusion and transport along geomagnetic field lines produced by thermospheric winds through neutral-ion collisions and (2) the zonal and meridional electromagnetic plasma drift. It should be noted that this feature and processes must always be taken into account in first-principle models for adequate description of the longitudinal and UT variations in ionospheric and plasmaspheric electron density. GSM TIP model has already been used to study: the longitudinal and UT variations of equatorial electrojet [*Klimenko et al*., 2007]; midlatitude and subauroral anomalies in F_2 layer peak electron density in separated longitudes [*Klimenko et al*., 2015a, 2015b]; the magnitude of longitudinal and LT variation in f_oF_2 and TEC [*Klimenko et al*., 2016a]; and the longitudinal variations of N_mF_2 in different latitudinal regions [*Klimenko et al*., 2016b]. We tried to identify the main morphological features of the longitudinal and LT variations in F_2 layer peak electron density and ionospheric and total electron content during 2009 northern winter solstice during solar activity minimum. For this reason the GSM TIP runs were carried out for quiet solstice conditions on 22 December 2009 without taking into account mesospheric tides on the lower boundary of the model (80 km).

4. IRTAM and NeQuick Brief Description

We used also empirical and assimilative models of the ionosphere to calculate reference values of the ionospheric electron density.

The first model is the IRI-based Real-Time Assimilative Mapping (IRTAM) [*Galkin et al*., 2012]. The IRTAM uses measurements from the Global Ionospheric Radio Observatory (GIRO) in combination with empirical knowledge of the ionospheric climate provided by the International Reference Ionosphere (IRI) model for the global ionospheric weather nowcast. GIRO is worldwide ionosonde network that currently includes over 80 ionosondes, of which about 50 stations provide near real-time data reports every 15 min. Every 15 min, in real time, the IRTAM smoothly transforms ("morphs") the IRI model prediction into agreement with the GIRO measurements using non-linear error compensation technique for associative restoration [*Galkin et al*., 2015] so that the new model representation closely follows the ionospheric weather variability. For IRTAM, relative simplicity of the underlying model formalism in comparison to the first-principle models has allowed 4DDA computations to span past history of model-versus-observation behavior for up to 24 h. The 4DDA stands for four-dimensional data assimilation: a class of assimilation techniques that use not only the latest data but also a history of past observations at each update step of the assimilation process (thus, it is 3-D plus 1-D time). By using 24 h history of observations rather than one latest measurement we ensure IRTAM robustness to data gaps and autoscaling errors.

The IRTAM assimilates available GIRO data by smooth modifications of the underlying IRI maps of the density profile anchor points (f_oF_2, h_mF_2) into a better agreement with the observations. Both f_oF_2 and h_mF_2 global maps for IRI and IRTAM are built using the same Jones-Gallet formalism [*Jones and Gallet*, 1962]. The underlying IRI model is configured to use URSI-88 coefficients for f_oF_2 [*Rush*, 1992] and coefficients for h_mF_2 [*Brunini et al*., 2013] (which is not the standard option of the original IRI). IRTAM uses the same formalism to represent every ionospheric parameter (foF_2, h_mF_2, etc.) and calculate updated representation (coefficient set) separately for each of them. Magnetic field is accounted in IRTAM (as well as in IRI) by the use of International Reference Magnetic Field (IGRF) model. Thus, IRTAM accounts for precise position of the magnetic equator that is important to accurately reproduce ionospheric features at low magnetic latitudes. A 12 month running mean sunspot number, Rz_{12}, does not have role of the driver for IRTAM modeling (it plays important role in IRI), since all effects due to solar activity are "built-in" observational data. In the regions far away (more than 1500 km) from GIRO ionosondes IRTAM modeling results are close to IRI results. Within the 1500 km distance from GIRO ionosonde locations, the IRTAM improvement of IRI climatology is on average twofold for a quiet time ionosphere, and more than threefold during the periods of disturbed ionosphere and in some other particular cases. IRTAM uses only three components: IRI climatology representation, IGRF magnetic field representation, and observational data to do the computations. Thus, IRTAM provides reliable specification of the ionospheric weather, given good data coverage.

However, IRTAM does not provide the entire electron density profile specification yet, pending implementation of the profile shape parameter mapping algorithms, which is the reason why NeQuick 2 empirical model is used for TEC/IEC representations. The NeQuick 2 model is a three-dimensional and time-dependent ionospheric electron density model [*Radicella and Leitinger*, 2001; *Nava et al*., 2008]. The model of the topside electron density profile is represented by a semi-Epstein layer where thickness is with empirically determined height-dependent thickness parameter [*Coïsson et al*., 2006]. NeQuick 2 model is able to provide the electron density and TEC values at different altitudinal regions up to 20,200 km.

5. Results and Discussion

In this section, we present a comparison of the GSM TIP numerical simulation results, IRTAM nowcasting and NeQuick computations with different kinds of satellite measurements. All data correspond to the period of December 2009 to January 2010. We performed different integration, as discussed above, to study the spatial and temporal morphological features. As assimilative model, IRTAM is driven by the measurements of the GIRO ionosonde network. The spatial coverage of data for December 2009 is better for the Northern Hemisphere than for the Southern Hemisphere. Thus, the quality of the IRTAM maps is better in the Northern Hemisphere and the IRTAM maps for the Southern Hemisphere should be analyzed with some cautions.

Figure 1 shows the N_mF_2, IEC, and TEC variations as a function of LT and geographic longitude variability (latitude integrated maps). These maps are referred as diurnal variations and produced as follows: (1) we calculate 24 (1 h resolution) global maps with the spatial resolution of 15° by longitude and 5° by latitude for particular local time; (2) we integrate over latitude and join all longitudinal profiles according to local time (for given longitude and UT we can uniquely find LT); and (3) finally, we normalize every map to a maximal

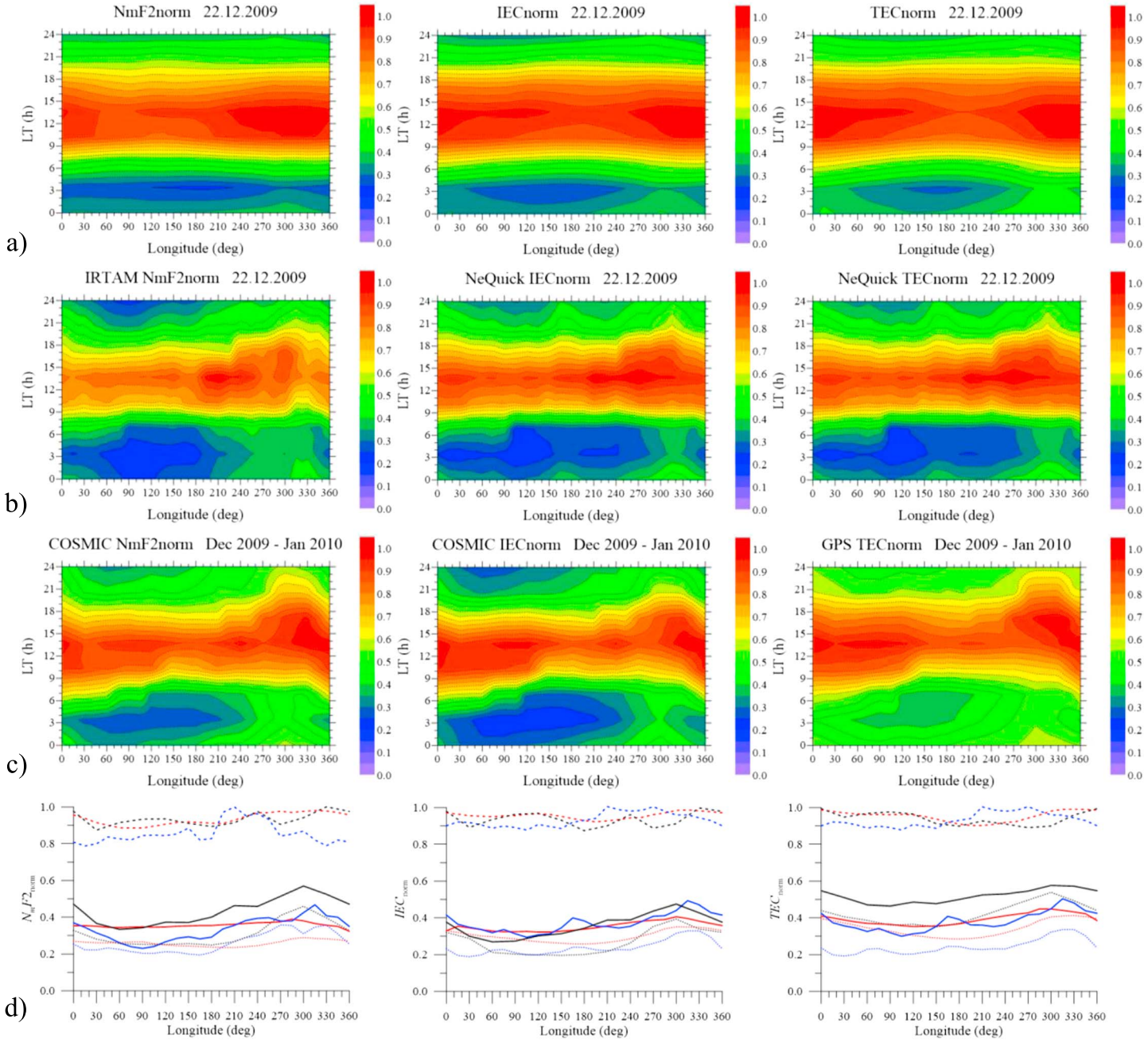

Figure 1. Longitudinal variations of the normalized N_mF_2 (left column), IEC (middle column), and TEC (right column) at the different local times. Maps are presented as a function of longitude and LT. Data are integrated over latitude for 22 December 2009. Maps display the normalized N_mF_2, IEC (from height of 80 km up to 700 km) and TEC (from height of 80 km up to 20,200 km) variations as shown by (a) GSM TIP; (b) IRTAM N_mF_2 and NeQuickIEC and TEC computations; (c) and COSMIC N_mF_2 and IEC observations and GPS TEC ground-based receivers measurements. (d) In addition, the longitudinal profiles of all these normalized parameters obtained using GSM TIP (red color), IRTAM and NeQuick models (blue color), and COSMIC and GPS observations (black color) at 14:00 LT (dashed lines), 24:00 LT (solid lines), and 04:00 LT (dotted lines) are presented.

value contained in this map. We can see the LT dependence of longitude variations according to all three used models in general is in a good agreement with the observations. However, there is a distinct difference between the GSM TIP and either IRTAM or NeQuick in terms of a correspondence to the COSMIC or GPS data: (1) in general, the GSM TIP presents lesser longitudinal variation than either IRTAM or NeQuick; and (2) the GSM TIP model results have a broader daytime LT extent in comparison to the empirical model. It is also notable that the nighttime normalized GPS TEC remains higher in comparison to the NeQuick (distinctly) and GSM TIP (insignificantly) model results, which is an indication of the plasmasphere effect [*Lunt et al.*, 1999a;

Mazzella, 2009]. These results show that (1) the empirical and numerical models represent adequately the longitudinal variations of N_e and TEC, which agree with our earlier studies [*Klimenko et al*., 2015a, 2015b]; and (2) the main reason for a longitude variation is the misalignment of the geographic and geomagnetic axis accounted in all three models. In our opinion, the main reason that the GSM TIP shows lesser longitudinal variation in comparison to the NeQuick and GPS map-derived TEC could be a usage of a simplified dipole geomagnetic field model in the GSM TIP instead of the IGRF model in IRTAM and NeQuick models. In addition, the GSM TIP computes the longitudinal variations without accounting for the mesospheric tides in the GSM TIP model simulations, which are an important source of the longitudinal variations in the ionospheric electron density. The magnitude of longitudinal variations is larger at night compared to noontime and morning time in both model computations and observational data. The evening longitudinal variations of electron density may be even larger than the nighttime variations according to IRTAM and NeQuick empirical models, COSMIC, and GPS observations. The main distinct difference of the magnitude of longitudinal variations in the electron density between GSM TIP and either IRTAM or NeQuick, in terms of their matching of the COSMIC or GPS data, appears during the evening hours. This can be explained by absence in the description of the GSM TIP model such phenomena as the *F* region dynamo electric field, mesospheric tides, and South Atlantic Anomaly in magnetic field. The notable data features, such as the LT at which the N_mF_2/IEC/TEC maxima occur as a function of longitude, or the temporal scales associated with the density enhancements depict some differences between observations and the GSM TIP model results. An important feature that the GSM TIP model is yet to reproduce is the higher magnitude of the longitude variations during evening hours versus the morning time. Probable mechanism for formation of this feature is prereversal enhancement. GPS TEC maps for December 2009 to January 2010 indicate an occurrence of the prereversal enhancement influence on the low-latitude TEC structure (see supporting information) that is absent in the GSM TIP TEC maps. Distinctly different longitudes of the maxima appear to disagree more between the models and the data than between the different quantities (N_mF_2, IEC, and TEC). The data maxima (COSMIC or GPS) appear to be near 330° longitude, while the NeQuick maxima (IEC and TEC) appear to be near 270° longitude, the IRTAM N_mF_2 maximum appears to be near 210° longitude, and the GSM TIP maxima in IEC, TEC, and N_mF_2 appear to be broadly spread around 330° longitude. We note a close resemblance between the NeQuick-derived IECnorm and TECnorm results, which can be explained by the fact that the NeQuick model has not a specific plasmasphere model and uses a simplified extension of the electron density profile toward the altitudes above 20,000 km. That is why the NeQuick TEC reproduces the same features as the NeQuick IEC. The NeQuick model performance on the topside electron content representation, including analysis of the absolute TEC values for the December 2009 conditions, was discussed by *Cherniak and Zakharenkova* [2016].

Figure 2 presents the N_mF_2, IEC, and TEC variations as a function of longitude and latitude (time integrated maps). These maps are referred as latitude variations and produced as follows: (1) we calculate 24 (1 h resolution) N_mF_2, IEC, and TEC global maps with a spatial resolution of 15° by longitude and 5° by latitude for each UT hour; (2) we integrate over time (LT or UT, it does not matter since we consider 24 h time interval) at the same longitude; and (3) finally, we normalize every map to a maximal value of this map. Polar ionospheric cavity and the main ionospheric trough are the major features seen in the high-latitude region of the Northern Hemisphere as equatorward as ~55°N. We note that it is difficult to discern the polar ionospheric cavity and the main ionospheric trough as distinct features in the N_mF_2 contour panels of Figure 2, so a detailed analysis of the N_mF_2 latitudinal structure (see supporting information) together with morphological position of the polar ionospheric cavity and main ionospheric trough according to *Brinton et al*. [1978] and *Benson and Grebowsky* [2001] was applied in order to identify these features. Both GSM TIP and IRTAM depict these features, which are also in agreement with the COSMIC observations. The GSM TIP appears to match the COSMIC data more closely in the northern polar region in comparison to the IRTAM results. Polar ionospheric cavity appears at 290°E and 270°E longitude in GSM TIP and IRTAM maps, correspondingly, and it is more pronounced in the GSM TIP map rather than in the IRTAM map. The main ionospheric trough appears to have a minimum at 75°N according to all considered data sets, but at slightly different longitudes: 120°E as modeled by GSM TIP; 60°E as mapped by IRTAM; 60°E as mapped by COSMIC. The GSM TIP longitudinal profiles for N_mF_2 and IEC at 75°N appear to be quite similar to each other. The ionospheric vertical profile of electron density at 75°N latitude is formed by only O^+ ions due to the O^+/H^+ transition height, located much higher than 700 km. In addition, the main role in the diffusive distribution of electron density at heights

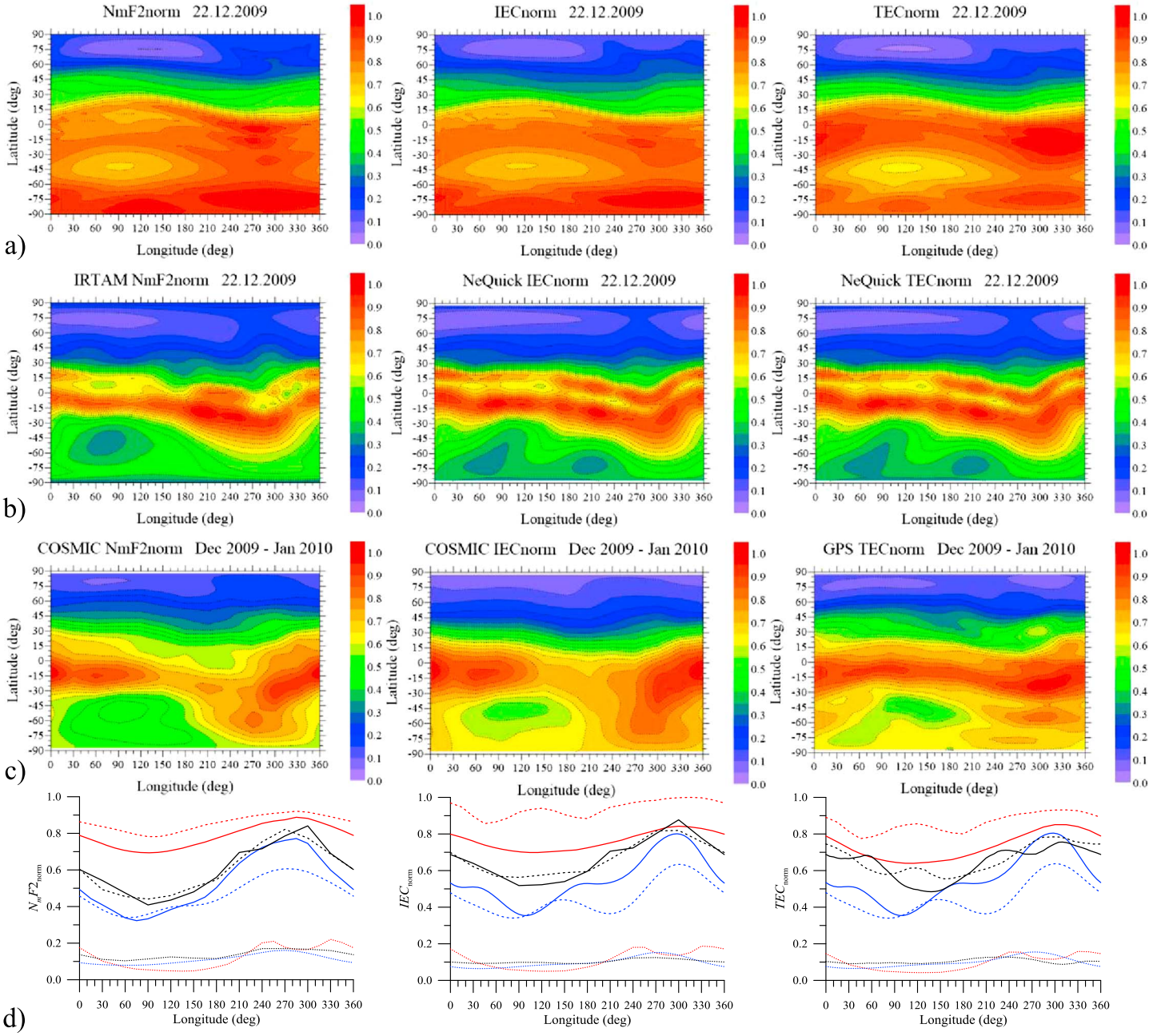

Figure 2. The same as in Figure 1 but at different latitudes. Maps are presented as a function of longitude and latitude. The longitudinal profiles of all normalized parameters obtained using the GSM TIP (red color), IRTAM and NeQuick models (blue color), and COSMIC and GPS observations (black color) at 60°S (dashed lines), 45°S (solid lines), and 75°N (dotted lines) are presented in Figure 2d.

of the *F* region and topside ionosphere does not play processes of the vertical plasma transport but the uniform horizontal plasma transport due to electromagnetic drift. These two reasons lead to the qualitatively similar latitude-longitude distribution of electron density at different heights of the *F* region and topside ionosphere at high latitudes. At all latitudinal regions the GSM TIP model results show one or two peaks in the N_mF_2 and IEC longitudinal distribution, but the IRTAM N_mF_2 and NeQuick IEC show several such peaks. This discrepancy can be caused by the limitations of the models. On one hand, the GSM TIP accounts for the magnetic field as for the simple dipole-like field and also it does not take into account the mesospheric tides. On the other hand, the IRTAM depends on data coverage. Ionosondes in the Northern Hemisphere are concentrated mainly in the three sectors: North American, European, and Asian. Hence, the observed

maximum might be an artifact of the nonuniform data coverage. It could be also noted that the COSMIC results appear to more closely resemble to the corresponding IRTAM and NeQuick results in comparison to the GSM TIP model output. We also note differences in the representation of the northern (winter) crest of the equatorial ionization anomaly between the COSMIC and IRTAM results, which could be explained by the facts: (1) definitely, a number of COSMIC RO profiles with F_2 peak values appeared exactly within a narrow band of the equatorial ionization anomaly northern crest during December–January are rather small; (2) Abel inversion technique assumed a spherical symmetry of the ionosphere, which, in fact, is far from reality in the equatorial region; that is why a proper reproduction of the crest-trough-crest structure in the presence of the large plasma density gradients could be rather problematic and it is a well-known issue for the RO measurements [e.g., *Pedatella et al*., 2015].

Also, GSM TIP, NeQuick, and IRTAM show the most pronounced equatorial anomaly crests nearly in the same longitudinal region: (240°E–300°E) for the GSM TIP and NeQuick and (210°E–270°E) for the IRTAM. The modeled position of maxima and minima of longitudinal variability of the F_2 peak electron density at the midlatitudes of the Southern Hemisphere also shows a good agreement with the COSMIC observations. The magnitude of this longitudinal variability is much lesser in the GSM TIP model in comparison with the observation data and the IRTAM model results. The summer midlatitudinal minimum of the N_mF_2 distribution is located at (45°S, 90°E), and its maximum is located in the longitudinal range of 220°E–330°E that coincides with a longitudinal position of the midlatitude summer nighttime/evening anomaly and the Weddell Sea Anomaly (WSA) [*Lin et al*., 2010; *Liu et al*., 2010; *Klimenko et al*., 2015a, 2015b] in the Southern Hemisphere. The main difference between the GSM TIP and either the IRTAM or NeQuick simulations appears in the high-latitude region of the Southern Hemisphere. The GSM TIP model depicts the local high-latitude maximum at (75°S, 300°E) that is also slightly visible according to the COSMIC observation; however, IRTAM and NeQuick do not demonstrate the same feature. We can explain this by the insufficient data coverage in the region. The maximum in the longitudinal variation of N_mF_2 and IEC in the Southern Hemisphere is located in the American longitudinal sector. The latitudinal structure of the ionospheric plasma maximum in the American longitudinal sector is more complex as simulated by the GSM TIP and observed by the COSMIC, rather than IRTAM and NeQuick (Figure 2).

Figure 3 shows the normalized N_e values on a longitude-latitude (geographic) grid. N_e corresponds to the different altitude: ~480 km (left), maps are based on the GRACE observations and ~300 km (right), maps are based on the CHAMP-derived in situ observations (Figure 3b); 480 km, maps are based on the GSM TIP results and are integrated over local time intervals of 23:00–04:00 LT and 13:00–18:00 LT that consists of the temporal intervals of the GRACE measurements (Figure 3c, left); 300 km, maps are also based on the GSM TIP results and are integrated over local time intervals of 06:00–11:00 LT and 17:00–22:00 LT that consists of temporal intervals of the CHAMP measurements (Figure 3c, right); the same as Figure 3c but integrated over 24 h (Figure 3d). Basically, Figure 3d (left and right) shows the same picture as corresponding to Figure 3c (left and right) and we provide both of them for a reference. Figure 3a shows a distribution of the measurements quantity for GRACE and CHAMP data on the left and right, respectively. Measurement number is integrated over a latitude, and thus, Figure 3a shows an amount of data under investigation for a particular LT and longitude. The reason for having Figure 3c along with Figure 3d is that Figure 3c follows the CHAMP and GRACE observations availability, and thus, it is more rationally to compare Figure 3b with Figure 3c than with Figure 3d.

The TEC longitudinal variations as modeled by the GSM TIP and shown by observations are agree in general with each other. One model/observations discrepancy is that the high-latitude summer maximum in the GPS TEC appears at ~60°S in observations and at ~75°S in the GSM TIP results (Figure 2, right column). It is necessary to note that low coverage of GPS TEC data at high-latitudes of the Southern Hemisphere makes it harder to identify this density enhancement feature reliably. Another issue is about the relative distribution of N_mF_2 (Figure 2, left column) and TEC in the high-latitude region of the Southern Hemisphere and in the equatorial region. Plasma density in the Southern Hemisphere is greater than that in the Northern Hemisphere, which is reasonable since the Southern Hemisphere is subjected to more solar ionizing radiation (December corresponds to the local summer condition in the Southern Hemisphere). However, we can see that N_mF_2 and TEC are even higher at high latitudes of the Southern Hemisphere than in the low-latitude and equatorial ionosphere. In our opinion, a nature of the high values of N_mF_2 and TEC at the high latitudes of the

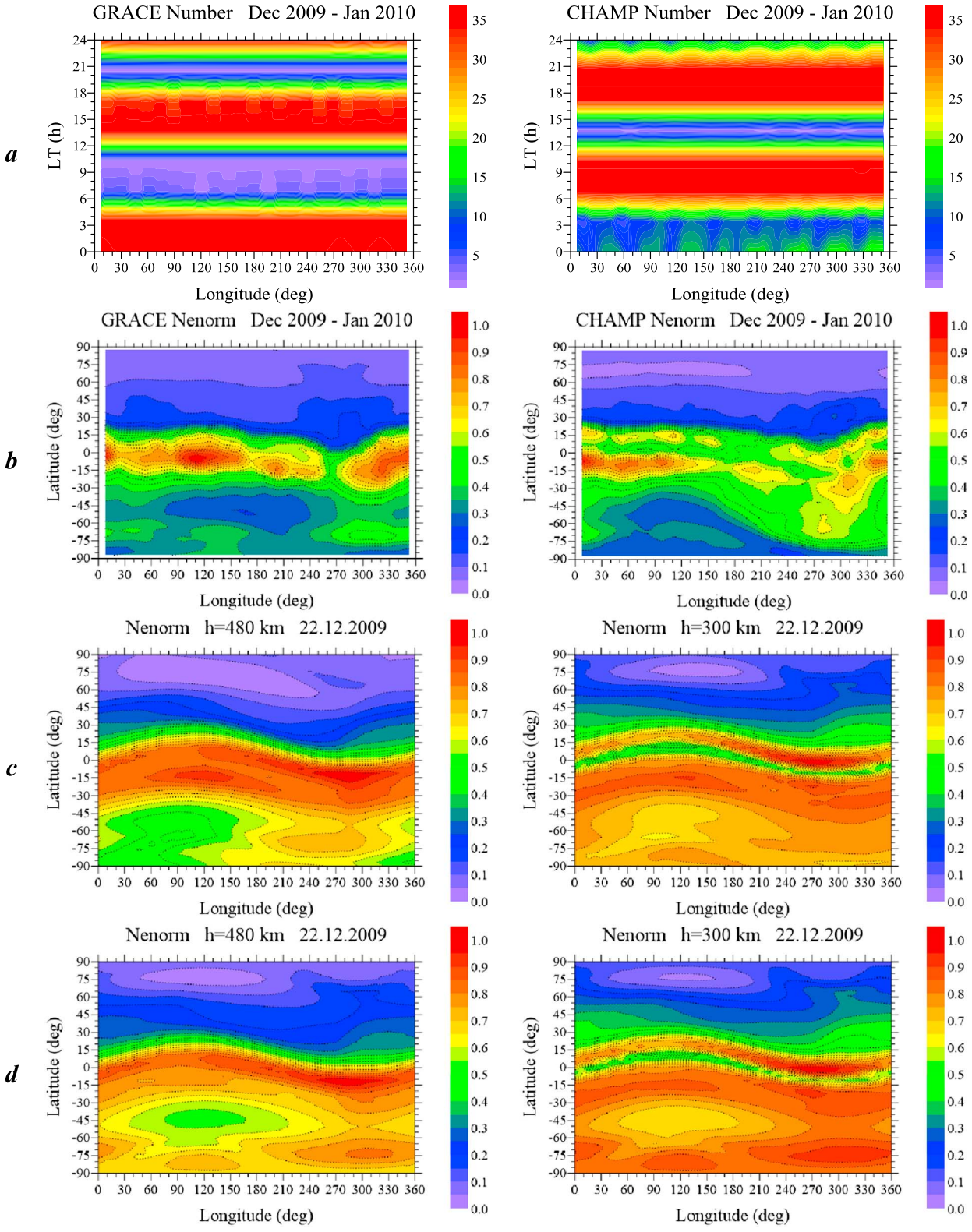

Figure 3. Longitude variations of the normalized electron density N_e at an altitude of ~480 km (left column) and ~300 km (right column) at different latitudes. Maps show the normalized N_e on longitude-latitude grid. Data are accumulated for December 2009 to January 2010. (a) The number of N_e measurements from GRACE (left) and CHAMP (right) satellites in the different LT epochs at different longitudes, integrated over a latitude; (b) normalized N_e variations as derived from the GRACE (left) and CHAMP (right) observations; (c) normalized N_e variations by GSM TIP computations integrated over local time in the time interval 23:00–04:00 LT and 13:00–18:00 LT at altitude of 480 km (left) and 06:00–11:00 LT and 17:00–22:00 LT at altitude of 300 km (right); (d) the same as Figure 3c but integrated over 24 h.

Southern Hemisphere is a "polar day," i.e., solar ionizing radiation throughout the whole day. This result should be subjected for further study, and it is not discussed in detail in this paper. Here we perform only the qualitative comparison. We expect that the high-latitude TEC maximum in the American longitude sector as seen by the GPS observations and reproduced by the GSM TIP (Figure 2, right column) should yield the similar maximum in N_mF_2 (Figure 2, left column). Indeed, such a maximum in N_mF_2 forms over the same region as shown by the GSM TIP data and COSMIC observations, but it is absent in the IRTAM and NeQuick maps, which again can be attributed to the insufficient data coverage.

Finally, we attempted to verify an existence of this high-latitudinal maximum using the CHAMP (~300 km) and GRACE (~480 km) in situ electron density measurements for the same time epoch (Figure 3). Independent measurements on board the CHAMP and GRACE satellites prove that this maximum is a real feature. The maximum seems to be more pronounced in the topside ionosphere (GRACE observations) than closer to the F_2 layer peak (CHAMP observations). However, we cannot be absolutely sure since the CHAMP and GRACE observations are related to a different local time. We plot a number of both GRACE and CHAMP samples as a function of LT and longitude grid (integrated over latitude). According to Figure 3a, GRACE data corresponded mostly to daytime and nighttime LT, whereas CHAMP data corresponded to morning and evening times. *Klimenko et al*. [2016a] concluded that local time distribution of observations defines mainly the features of the latitude-longitude variations. The maximum, that we consider, is obviously related to the WSA maximum from ~23 LT to ~04 LT, and, hence, the GRACE observations depicted it more clearly. *Zakharenkova and Cherniak* [2015] indirectly confirmed this assumption using the GOCE and TerraSAR-X satellite GPS observations. They showed that the high-latitude maximum did not appear during evening hours (17:00–18:00 LT) and only slightly appeared at morning hours (05:00–06:00 LT). To check our assumption we integrated the GSM TIP results: (1) for the whole day (over all 24 h) at the heights of CHAMP and GRACE satellites (Figure 3d) and (2) only during 23:00–04:00 LT and 13:00–18:00 LT at height of ~480 km and 06:00–11:00 LT and 17:00–22:00 LT at height of ~300 km (Figure 3c). We can note that the aforementioned maximum is depicted clearly at every map.

6. Summary

We have analyzed the major morphological features that characterize latitudinal, longitudinal, and LT variations of N_mF_2/IEC/TEC for the December 2009 solstice. Intercomparison of TEC, IEC (ionospheric electron content from 80 to 700 km), and N_mF_2 data demonstrates that they are overall similar. However, locations and magnitudes of their longitudinal features, as seen at different latitudes and LT, can be different. There are many publications where people try to convert the vertical TEC derived from much more dense GPS networks than the ionosonde one into the absent N_mF_2 values using very simple formulas [*Houminer and Soicher*, 1996; *Krankowski et al*., 2007; *Yu et al*., 2013; *Maltseva and Mozhaeva*, 2015]. We wanted to stress that our results do not support correctness of such simple conversion between N_mF_2/IEC/TEC. We emphasize that according to the first-principle, empirical, and assimilation models, as well as satellite observations, the longitudinal maxima in N_mF_2, IEC, and TEC are formed at all local times and at almost all latitudes (summer Southern Hemisphere and midlatitude and high latitude in winter Northern Hemisphere) in the American/Atlantic longitudinal sector (240–360°). The plasma density in the ionosphere is generally greater in the American longitudinal sector at any LT epoch. We can distinguish the near-equatorial and high-latitude maxima for all three parameters in this longitudinal sector. High-latitude maximum over the American longitudinal sector appears in the GSM TIP and COSMIC N_mF_2 and IEC; GSM TIP, CHAMP, and GRACE N_e; and GSM TIP and GPS TEC but does not appear in the NeQuick and IRTAM results. The local maximum in the Atlantic/American sector is related to the WSA manifestation. The most probable reason of the absent or weak WSA effects in the IRTAM, as well as NeQuick, is that only one ionosonde (Port Stanley located at the Falkland Islands) operates routinely now in the whole southeastern Pacific and southwestern Atlantic region. So lack of actual measurements does not allow to reproduce signatures of the WSA at middle and high latitudes of the South American sector in the ionosonde data or ionosonde-based empirical models. What we can conclude about this local maximum now? According to our results, the high-latitude maximum of N_mF_2 (1) manifests itself only when the integration over LT or UT of global maps for 22 December 2009 includes nighttime, thus supporting an argument of its association with the Weddell Sea Anomaly, and (2) also appears in N_e distribution at heights above the F_2 peak. We would recommend an inclusion of this maximum for building of an accurate empirical model of the quiet time ionosphere.

Acknowledgments
We acknowledge GFZ Potsdam for providing CHAMP PLP and GRACE KBR data through the ISDC data center (http://isdc.gfz-potsdam.de/). We are grateful to the Taiwanese National Space Organization and the University Corporation for Atmospheric Research for providing the FORMOSAT-3/COSMIC data (http://cdaac-www.cosmic.ucar.edu/cdaac/) and to the International GNSS Service (IGS) for providing GIM products via the Crustal Dynamics Data Information System (CDDIS) at the NASA Goddard Space Flight Center FTP site (ftp://cddis.gsfc.nasa.gov/pub/gps/products/ionex/YYYY/DDD/IGSGDDD0.YYi). IRTAM model results were retrieved from the GAMBIT database operated by Lowell GIRO Data Center (http://giro.uml.edu/GAMBIT) using GAMBIT Explorer software. GSM TIP model results are available from the authors upon request. We acknowledge the Telecommunications/ICT for Development (T/ICT4D) Laboratory of the Abdus Salam International Centre for Theoretical Physics, Trieste, Italy, for providing NeQuick-2 model (http://t-ict4d.ictp.it/nequick2/nequick-2-web-model). This study was financially supported by grants from RFBR 15-35-20364 and 14-05-00788 and within the project "Physical mechanisms of the reaction of the upper atmosphere and ionosphere on the processes in the lower atmosphere and on the Earth surface" (State task Education and Science Ministry of the Russian Federation, the competitive part of the task 3.1127.2014/K). The authors thank one anonymous reviewer and Andrew Mazzella for their constructive comments, which improved greatly this paper.

References

Afraimovich, E. L., E. I. Astafyeva, E. A. Kosogorov, and Y. V. Yasyukevich (2011), The mid-latitude field-aligned disturbances and its impact on differential GPS and VLBI, *Adv. Space Res.*, *47*, 1804–1813, doi:10.1016/J.ASR.2010.06.030.

Benson, R. F., and J. M. Grebowsky (2001), Extremely low ionospheric peak altitudes in the polar hole region, *Radio Sci.*, *36*(2), 277–285, doi:10.1029/1999RS002401.

Bilitza, D., and B. W. Reinisch (2008), International Reference Ionosphere 2007: Improvements and new parameters, *Adv. Space Res.*, *42*(4), 599–609, doi:10.1016/J.ASR.2007.07.048.

Brinton, H. C., J. M. Grebowsky, and L. H. Brace (1978), The high-latitude winter F region at 300 km: Thermal plasma observations from AE-C, *J. Geophys. Res.*, *83*, 4767–4776, doi:10.1029/JA083iA10p04767.

Brunini, C., J. F. Conte, F. Azpilicueta, and D. Bilitza (2013), A different method to update monthly median h_mF_2 values, *Adv. Space Res.*, *51*(12), 2322–2332.

Cherniak, I., and I. Zakharenkova (2016), NeQuick and IRI-Plas model performance on topside electron content representation: Spaceborne GPS measurements, *Radio Sci.*, *51*, 752–766, doi:10.1002/2015RS005905.

Cherniak, I. V., I. E. Zakharenkova, A. Krankowski, and I. I. Shagimuratov (2012), Plasmaspheric electron content derived from GPS TEC and FORMOSAT-3/COSMIC measurements: Solar minimum conditions, *Adv. Space Res.*, *50*(4), 427–440, doi:10.1016/J.ASR.2012.04.002.

Cherniak, I. V., I. E. Zakharenkova, D. Dzubanov, and A. Krankowski (2014), Analysis of the ionosphere/plasmasphere electron content variability during strong geomagnetic storm, *Adv. Space Res.*, *54*(4), 586–594, doi:10.1016/j.asr.2014.04.011.

Clilverd, M. A., N. P. Meredith, R. B. Horne, S. A. Glauert, R. R. Anderson, N. R. Thomson, F. W. Menk, and B. R. Sandel (2007), Longitudinal and seasonal variations in plasmaspheric electron density: Implications for electron precipitation, *J. Geophys. Res.*, *112*, A11210, doi:10.1029/2007JA012416.

Coïsson, P., S. M. Radicella, R. Leitinger, and B. Nava (2006), Topside electron density in IRI and NeQuick: Features and limitations, *Adv. Space Res.*, *37*(5), 937–942, doi:10.1016/j.asr.2005.09.015.

Eccles, D., J. W. King, and P. Rothwell (1971), Longitudinal variations of the mid-latitude ionosphere produced by neutral-air winds—II. Comparisons of the calculated variations of electron concentration with data obtained from the Ariel I and Ariel III satellites, *J. Atmos. Terr. Phys.*, *33*(3), 371–377.

Galkin, I. A., B. W. Reinisch, X. Huang, and D. Bilitza (2012), Assimilation of GIRO data into a real-time IRI, *Radio Sci.*, *47*, RS0L07, doi:10.1029/2011RS004952.

Galkin, I. A., A. M. Vesnin, X. Huang, A. V. Kozlov, P. Song, and B. W. Reinisch (2015), GAMBIT database and explorer for real-time IRI maps of F_2 layer peak height and density 14th IES-2015 Proceedings, 8 pp., Alexandria, Va., 12–14 May.

Houminer, Z., and H. Soicher (1996), Improved short-term predictions of f_oF_2 using GPS time delay measurements, *Radio Sci.*, *31*(5), 1099–1108, doi:10.1029/96RS01965.

Jones, W. B., and R. M. Gallet (1962), Presentation of diurnal and geographical variations of ionospheric data by numerical methods, *ITU Telecommun. J.*, *29*(5), 129–149.

Klimenko, M. V., V. V. Klimenko, and V. V. Bryukhanov (2007), Numerical modeling of the equatorial electrojet UT-variation on the basis of the model GSM TIP, *Adv. Radio Sci.*, *5*, 385–392.

Klimenko, M. V., V. V. Klimenko, A. T. Karpachev, K. G. Ratovsky, and A. E. Stepanov (2015a), Spatial features of Weddell Sea and Yakutsk Anomalies in f_oF_2 diurnal variations during high solar activity periods: Interkosmos-19 satellite and ground-based ionosonde observations, IRI reproduction and GSM TIP model simulation, *Adv. Space Res.*, *55*(8), 2020–2032, doi:10.1016/J.ASR.2014.12.032.

Klimenko, M. V., V. V. Klimenko, K. G. Ratovsky, I. E. Zakharenkova, Y. V. Yasyukevich, N. A. Korenkova, I. V. Cherniak, and A. A. Mylnikova (2015b), Mid-latitude Summer Evening Anomaly (MSEA) in F_2 layer electron density and total electron content at solar minimum, *Adv. Space Res.*, *56*(9), 1951–1960, doi:10.1016/J.ASR.2015.07.019.

Klimenko, M. V., V. V. Klimenko, I. E. Zakharenkova, and I. V. Cherniak (2015c), The global morphology of the plasmaspheric electron content during Northern winter 2009 based on GPS/COSMIC observation and GSM TIP model results, *Adv. Space Res.*, *55*(8), 2077–2085, doi:10.1016/J.ASR.2014.06.027.

Klimenko, M. V., et al. (2016a), Diurnal and longitudinal variations in the Earth's ionosphere during solstice in a deep minimum of solar activity, *Cosmic Res.*, *54*(1), 10–22.

Klimenko, V. V., A. T. Karpachev, M. V. Klimenko, K. G. Ratovsky, and N. A. Korenkova (2016b), Latitudinal structure of longitudinal effect in nighttime ionosphere during summer and winter solstice condition, *Russ. J. Phys. Chem. B*, *35*(1), 21–30.

Krankowski, A., I. I. Shagimuratov, and L. W. Baran (2007), Mapping of f_oF_2 over Europe based on GPS-derived TEC data, *Adv. Space Res.*, *39*(5), 651–660.

Lin, C. H., C. H. Liu, J. Y. Liu, C. H. Chen, A. G. Burns, and W. Wang (2010), Midlatitude summer nighttime anomaly of the ionospheric electron density observed by FORMOSAT-3/COSMIC, *J. Geophys. Res.*, *115*, A03308, doi:10.1029/2009JA014084.

Liu, H., S. V. Thampi, and M. Yamamoto (2010), Phase reversal of the diurnal cycle in the midlatitude ionosphere, *J. Geophys. Res.*, *115*, A01305, doi:10.1029/2009JA014689.

Lunt, N., L. Kersley, and G. J. Bailey (1999a), The influence of the protonosphere on GPS observations: Model simulations, *Radio Sci.*, *34*(3), 725–732, doi:10.1029/1999RS900002.

Lunt, N., L. Kersley, G. J. Bishop, and A. J. Mazzella Jr. (1999b), The contribution of the protonosphere to GPS total electron content: Experimental measurements, *Radio Sci.*, *34*(5), 1273–1280, doi:10.1029/1999RS900016.

Maltseva, O., and N. Mozhaeva (2015), Obtaining ionospheric conditions according to data of navigation satellites, *Int. J. Antennas Propag.*, *2015*, 804791, doi:10.1155/2015/804791.

Mazzella, A. J., Jr. (2009), Plasmasphere effects for GPS TEC measurements in North America, *Radio Sci.*, *44*, RS5014, doi:10.1029/2009RS004186.

Namgaladze, A. A., Y. N. Korenkov, V. V. Klimenko, I. V. Karpov, F. S. Bessarab, V. A. Surotkin, T. A. Glushchenko, and N. M. Naumova (1988), Global model of the thermosphere-ionosphere-protonosphere system, *Pure Appl. Geophys.*, *127*(2/3), 219–254.

Nava, B., P. Coisson, and S. M. Radicella (2008), A new version of the NeQuick ionosphere electron density model, *J. Atmos. Sol. Terr. Phys.*, *70*(15), 1856–1862, doi:10.1016/J.JASTP.2008.01.015.

Pedatella, N. M., X. Yue, and W. S. Schreiner (2015), Comparison between GPS radio occultation electron densities and in situ satellite observations, *Radio Sci.*, *50*, 518–525, doi:10.1002/2015RS005677.

Radicella, S. M., and R. Leitinger (2001), The evolution of the DGR approach to model electron density profiles, *Adv. Space Res.*, *27*(1), 35–40, doi:10.1016/S0273-1177(00)00138-1.

Rush, C. M. (1992), URSI f_oF_2 model maps (1988), *Planet. Space Sci.*, *40*, 546–547, doi:10.1016/0032-0633(92)90181-M.

Xiong, C., J. Park, H. Lühr, C. Stolle, and S. Y. Ma (2010), Comparing plasma bubble occurrence rates at CHAMP and GRACE altitudes during high and low solar activity, *Ann. Geophys.*, *28*, 1647–1658, doi:10.5194/ANGEO-28-1647-2010.

Yu, Y., W. Wan, B. Zhao, Y. Chen, B. Xiong, L. Liu, J. Liu, Z. Ren, and M. Li (2013), Modeling the global N_mF_2 from the GNSS-derived TEC-GIMs, *Space Weather*, *11*, 272–283, doi:10.1002/SWE.20052.

Zakharenkova, I., and I. Cherniak (2015), How can GOCE and TerraSAR-X contribute to the topside ionosphere and plasmasphere research?, *Space Weather*, *13*, 271–285, doi:10.1002/2015SW001162.